DALAT UNIVERSITY JOURNAL OF SCIENCE Volume 11, Issue 1, 2021 68-79

SIMULATION OF XRF SPECTRA EMPLOYING A MODIFIED MCNP CODE

Nguyen Thi Tho[a*], Nguyen Kien Cuong[a], Huynh Ton Nghiem[a]

[a]Dalat Nuclear Research Institute, Lam Dong, Vietnam
[*]Corresponding author: Email: nguyenthoqn2002@yahoo.com

Article history
Received: June 30th, 2020
Received in revised form: November 15th, 2020 | Accepted: November 25th, 2020
Available online: February 5th, 2021

Abstract

The Monte Carlo N-Particle code (MCNP4C2 version) has been modified for atomic relaxation in both source code and library to simulate XRF spectra for different measurement configurations. The modified code was then used to simulate XRF spectra of six metal samples: Ni, Cu, Zn, Pd, Ag, Au, and Au alloys on an XRF spectrometer. The results are compared to those of experimental measurements. The intensity ratios of line pairs $K_{\beta 1}/K_{\alpha 1}$ and $L_{\beta 1}/L_{\alpha 1}$ between simulated and experimental values differ by about 4%-11% for the six single metals. The relative intensities of the Au alloys, compared to Au$L_{\alpha 1}$, were in the range of 0.02%-26.00%. The modified MCNP4C2 code is capable of forecasting the basic characteristics of new XRF designs.

Keywords: Atomic Relaxation; MCNP4C2; Monte Carlo Simulation; XRF Spectra.

DOI: http://dx.doi.org/10.37569/DalatUniversity.11.1.740(2021)

Article type: (peer-reviewed) Full-length research article

1. INTRODUCTION

Mathematical models are ineffective when solving problems of radiation transport for complex conditions of geometry, materials, and composition for radiation emitted from sources or generated during processing interactions. Monte Carlo simulation is the best solution for highly complex transport problems.

In X-ray fluorescence (XRF), Monte Carlo simulation is used as a method of quantitative analysis by creating synthetic spectra of standard samples that have the same matrix composition as the analyzed samples. The elemental concentration of the analyzed sample is determined by comparing its characteristic X-ray intensities to the standard sample. Vincze et al. (2004) used Monte Carlo simulation for homogenous and heterogeneous samples and obtained a deviation of 2%-15% compared to experiments. This method is especially effective for complex XRF geometry configurations.

The MCNP4C2 code has been used to simulate XRF spectra for different configurations at the Dalat Nuclear Research Institute. In the previous work, the atomic relaxation is only of concern as a small consequence of the photoelectric effect. It has not been the main purpose for simulating radiation transport. The MCNP code provides K-type transitions and only one <L>–<MN> average transition (Figure 1). This limitation of the algorithm and data library in the MCNP4C2 code has been analyzed and then supplemented to create a modified version for the XRF application. Figure 1 shows that the simulated (MCNP) spectrum is in good agreement with the experimental (Exp) spectrum of Cu-K lines, while in the case of Au-L lines, MCNP only showed an average line <L>–<MN>.

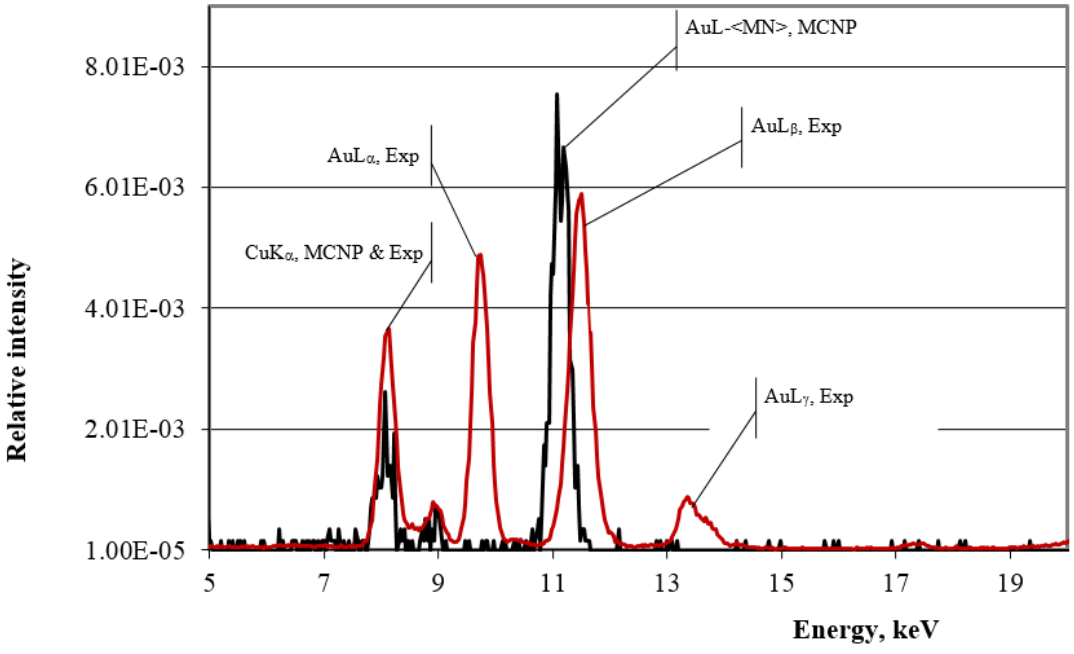

Figure 1. Comparison of simulated (MCNP) and experimental (Exp) spectra of a sample of Au-Cu alloy in an XRF configuration

The photoelectric effect occurs when a photon is absorbed during an interaction with an atom. The photon disappears, an e^- orbit separates from the atom and becomes e^- free (called a photoelectron) and leaves a vacancy. The atom stays in an excited state. In XRF, the photoelectric effect is considered for the atomic inner shells (K, L, M, N, etc) with energies of interest around 1-100 keV.

After the photoelectric process, the atom in the excited state returns to the ground state with transitions of e^- from weaker binding levels to the level having a vacancy (i.e., the transition vacancy returns to a weaker binding) and can emit characteristic X-rays. For example, a primary vacancy on the K shell can induce transitions K-L1 (Kα2), K-L3 (Kα1), K-M3 (Kβ1), K-N2/N3 (Kβ2), etc. Each of these transitions leaves a secondary vacancy at one of the upper levels and forms new transitions. Thus, a primary vacancy on the K shell, together with X-rays of the K group, will generate more X-rays at the L, M, etc groups. The same process occurs with primary vacancies in the upper levels.

2. ANALYSIS, COMPLEMENT OF ALGORITHM AND LIBRARY FOR RELAXATION OF MCNP

2.1. Analysis of algorithm and library

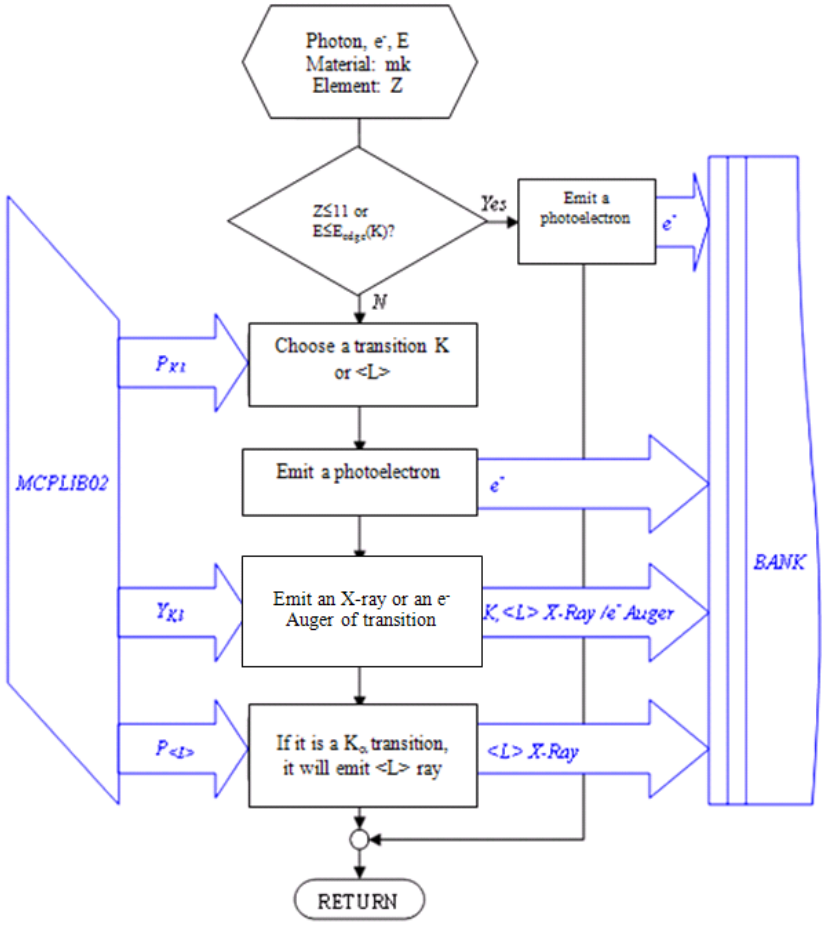

Figure 2. Algorithm flowchart of subroutine FLAUG, atomic relaxation simulation

In the MCNP4C2 code, the atomic relaxation process is performed in subroutine FLAUG. This subroutine is called by subroutine COLIDP for ionization by the photon or subroutine KXRAY for ionization by e^-. Subroutine FLAUG performs the atomic relaxation process by selecting one of the possible transitions with the probability listed in the library. This transition permits the emission of a fluorescent X-ray or an e^-Auger, depending on the fluorescence efficiency of the transition. The subsequent behavior of e^- Auger (modeled by subroutine ELECTR) allows the simulation of the radiative Auger phenomenon that is commonly seen in characteristic X-ray spectra.

To reduce computation time in the calculation of a photon's history, MCNP has simplified the ionization process. It only creates a primary vacancy on the K shell; the ionization phenomenon in the upper shells (L, M, N, etc) is neglected. The secondary transitions are reduced by simulating a <L> transition, which is a consequence of a secondary vacancy on the L shell when having a K-L (K_α) transition (Figure 2).

Corresponding to the FLAUG algorithm, the database for X-ray transitions of each element in the MCPLIB02 photon interaction library only contains K transitions and one <L>–<MN> transition (Figure 3).

		1/Jк	LX emission efficiency (cumulative)		
…Coherent Form Factors F(x,Z)					
Group L	0.013335	0.241	0	0	<L>-<MN>
	0.013335	1	0.2823	0.011125	
Group K	0.080725	2.941	2.13	0.068806	Kα1
	0.080725	4.079	3.213	0.066991	Kα2
	0.080725	4.712	3.816	0.077848	Kβ13
	0.080725	4.859	3.956	0.080146	Kβ24
	Absorbing edge, MeV	Transfer probability	X-ray emission efficiency	X-ray energies	
Heating number…					

Figure 3. Database for the X-ray transitions of element Au

The database can be described as a set of records, each record consisting of four data fields that characterize a transition, including absorbing edge, transfer probability $P_{K,l}$, X-ray emission efficiency $Y_{K,l}$, and X-ray energy of transition. The transfer probability and the emission efficiency are described in terms of cumulative probability for each group of X-rays, as

$$P_{K,l} = \sum_{i=1}^{l} p_{K,i}\ ,\ Y_{K,l} = \sum_{i=1}^{l} y_{K,i}\ ,\ y_{K,i} = \omega_K \cdot p_{K,i}\ , \tag{1}$$

where, ω_K is the K shell fluorescence yield, $p_{K,i}$ is the partial transition probability of an l^{st} transition to the K shell, and $y_{K,l}$ is the relative intensity of fluorescent X-ray K_l when having a primary vacancy on the K shell. This probability arrangement facilitates sampling to choose the transition.

The reduction of transition numbers causes MCNP to be unable to simulate XRF spectra, especially for large Z elements, which are often analyzed by L-rays.

2.2. Complement of algorithm and library for MCNP

For the purpose of describing the details of transitions of L shells and upper shells, subroutine FLAUG has supplemented the probability of forming the primary vacancy for all shells/grades-shells (K, L1, L2, L3, etc) of interest after photoelectric effects. Then, the relaxation is performed as in the original subroutine FLAUG for possible transitions of the selected primary vacancy (Figure 4).

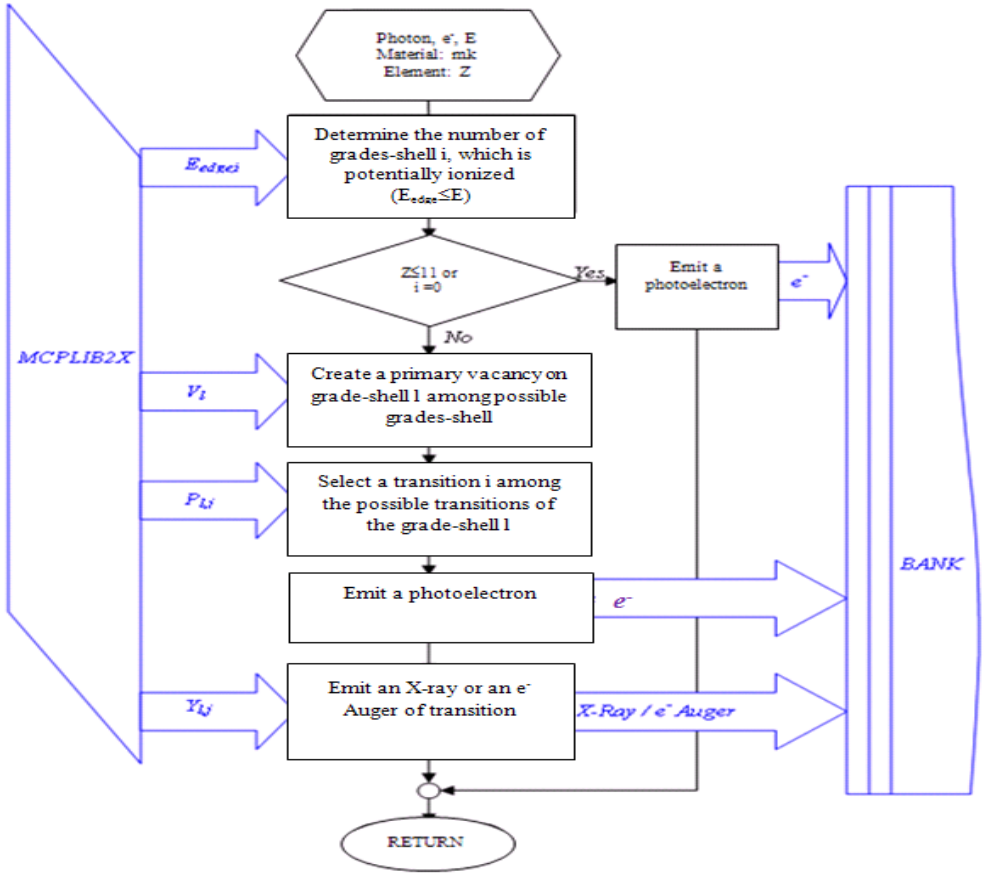

Figure 4. Algorithm flowchart of subroutine FLAUG with complemented consideration of primary vacancy formation after photoelectric effect

In response to the above change, the X-ray database of each nucleus in MCPLIB02 was also reorganized. The database consists of multiple partitions corresponding to the primary vacancy number to be considered. Each partition starts with a header record that stores the probability of forming the primary vacancy and the number of possible transitions of that vacancy (the number of records). Subsequent records store data for each transition, as in the original MCPLIB02. These modifications create a new photon interaction library, named MCPLIB2X (Figure 5).

	E_{edge}	Probability of primary vacancy $V_0(Z)$		Number of records	
…Coherent Form Factors F(x,Z)					
Vac. M and upper	0.0034249	0.061003	0	2	
	0.0034249	1	1	0	
Vacancy L3	0.01918	0.124396	0	7	L3 Header
	0.01918	0.6875	0.22	0.009713	L3-M5
	…	…	…	…	…
	0.01918	0.175398	0.31737	0.011916	L3-O4,O5
Vacancy L2	0.013733	0.115396	0	11	L2 Header
	0.013733	0.7994	0.267	0.011443	L2-M4
	...	…	…	…	…
	0.013733	1.11683	0.37302	0.011916	L3-O4,O5
Vacancy L1	0.014353	0.203425	0	15	L1 Header
	0.014353	0.420561	0.0490	0.01161	L1-M3
	…	…	…	…	…
	0.014353	3.064393	0.32789	0.011916	L3-O4,O5
Vacancy K	0.080723	911	0	25	L1 Header
	0.080723	0.4813278	0.646	0.068806	K-L3
	…	…	…	…	…
	0.080723	0.8779315	0.846325	0.077982	K-M3
	…	…	…	…	…
	0.080723	0.986791	0.951266	0.01161	L1-M3
	…	…	…	…	…
	Absorbing edge, MeV	Transfer probability	X-ray emission efficiency	X-ray energies	
Heating number…					

Figure 5. Arrangement of relaxation data for element Au in MCPLIB2X with data partitions for each primary vacancy

The primary vacancy probability of each grade-shell (*j, l*) is the ratio of the partial photoelectric cross-section $\tau_{jl}(E)$ and the total photoelectric cross-section $\tau(E)$: $v_{jl}(E) = \tau_{jl}(E) / \tau(E)$.

In principle, this probability depends on the incident photon energy. However, in this library, a constant probability calculated from the absorption jump values *kjl* is used. The *kjl* values were derived from the photon cross-section table of Veigele et al. (1971). In MCPLIB2X, these probabilities are also cumulative probabilities for convenient access. If arranged in order of binding energy, the calculated equations are as follows:

$$V_K = 1, V_{L1} = 1/k_K, V_{L2} = 1/(k_K . k_{L1}) \quad (2)$$

$$V_{L3} = 1/(k_K \cdot k_{L1} \cdot k_{L2}), V_{M1} = 1/(k_K \cdot k_{L1} \cdot k_{L2} \cdot k_{L3}) \quad (3)$$

In the energy range below 100 keV, the constant probability method usually gives correct results for K-rays, deviations < 2% for L_2 and L_3 transitions, and deviations < 10% for L1 transitions (Kawrakow & Roger, 2006).

The transition list for a primary vacancy has also been expanded, including secondary transitions on weaker link grades-shell due to the existence of a consecutive secondary vacancy (due to a secondary vacancy formed after a primary transition) and the substitution type formed by Auger and Coster-Kronig transitions. Data for the transition probability and fluorescent X-ray emission (intensity) efficiency of each transition were obtained from an online LBNL nuclear data library (LBNL Isotopes Project-Lunds Universitet) that was last updated in 2005.

3. SOME TEST APPLICATIONS AND EVALUATIONS

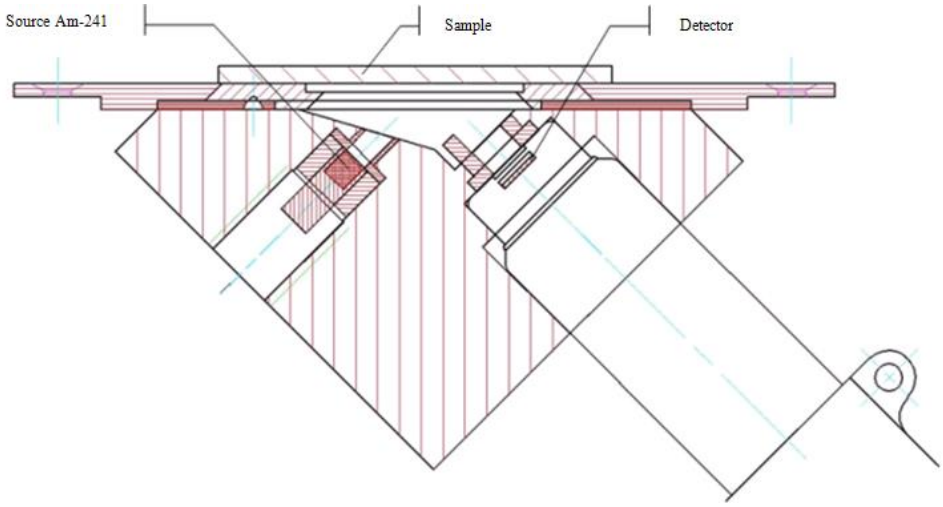

Figure 6. Description of the XRF configuration used in the survey

The modified version of the MCNP4C2 code was used to simulate the XRF spectra of six metal samples: Ni, Cu, Zn, Ag, Pd, Au, and Au alloys for an XRF spectrometer using a cylindrical ^{241}Am 100 mCi excitation source and a SiPIN detector with a crystal size of 5.0 mm × 5.0 mm × 0.5 mm. The XRF configuration is shown in Figure 6. In this work, AXIL software was used to analyze the simulated and experimental spectra.

The ^{241}Am source is a cylindrical ceramic pellet. The source is placed in a stainless steel cover with 0.5-mm thick walls and a 0.2-mm thick window. The ^{241}Am isotope decays by α emission to ^{239}Np, emits soft γ rays 59.536 keV (35.8%), 26.300 keV (2.4%), and NpLX rays (11.87-21.49 keV, 38.7%).

After passing through the stainless steel window, low energy photons (≤ 26.000 keV) are almost depleted. Therefore, the source energy is described as mono-energy with the 59.536 keV line to save computation time.

The effective sample size of the configuration is estimated to be 16.0 mm in diameter. The samples are made in disk form with a diameter of 18.0 mm and a thickness of 0.3 mm. The thickness is considered infinite for E ≤ 59.536 keV.

3.1. Simulation results of single-element samples

Table 1. Comparison of simulated and experimental intensity ratios for six elements

Intensity ratio	Simulation (MCPLIB02)		Simulation (MCPLIB2X)		Experiment (Exp.)		Difference	
	Value	Error	Value	Error	Value	Error	$\left(\frac{MCPLIB02-Exp}{Exp}\right)$	$\left(\frac{MCPLIB2X-Exp}{Exp}\right)$
Ni ($K_{\beta1}/K_{\alpha1}$)	0.252	0.005	0.250	0.005	0.261	0.004	-3.46%	-4.27%
Cu ($K_{\beta1}/K_{\alpha1}$)	0.248	0.007	0.248	0.005	0.272	0.004	-8.68%	-8.75%
Zn ($K_{\beta1}/K_{\alpha1}$)	0.239	0.005	0.238	0.004	0.269	0.003	-11.18%	-11.41%
Pd ($K_{\beta1}/K_{\alpha1}$)	0.117	0.006	0.150	0.003	0.165	0.004	-29.34%	-8.67%
Ag ($K_{\beta1}/K_{\alpha1}$)	0.140	0.005	0.148	0.003	0.165	0.004	-15.24%	-10.74%
Au ($L_{\beta1}/L_{\alpha1}$)			0.992	0.030	0.902	0.012		10.07%

The simulated spectrum is compared with the experimental one by the ratio of the peak pairs $K_{\beta1}/K_{\alpha1}$ ($L_{\beta1}/L_{\alpha1}$ for Au). In general, the deviation between the simulation and experiment was about 4%-11% (Table 1), which is almost no greater than the error of the relative intensity data of X-ray transitions used in library MCPLIB2X (LBNL Isotopes Project-Lunds Universitet, n.d.).

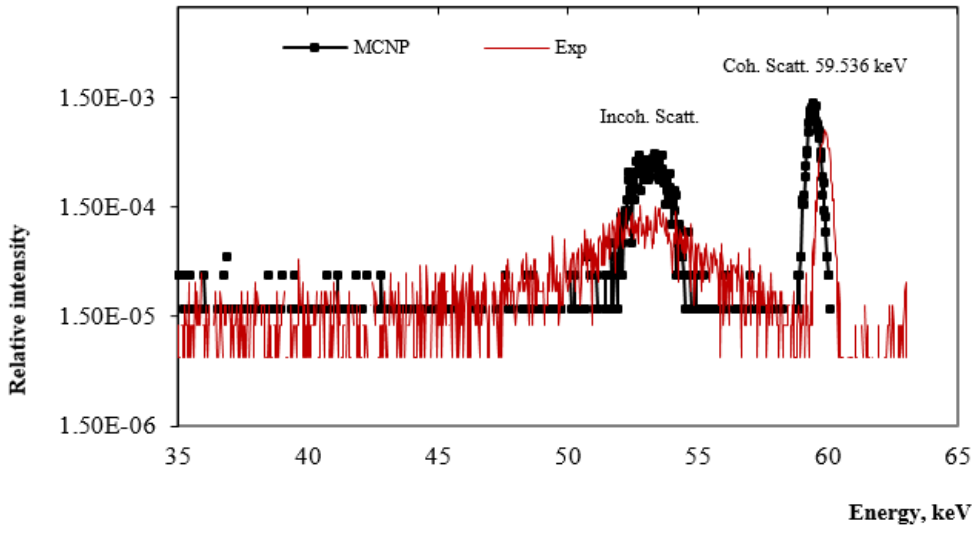

Figure 7. Comparison of simulated and experimental Compton scattering spectra

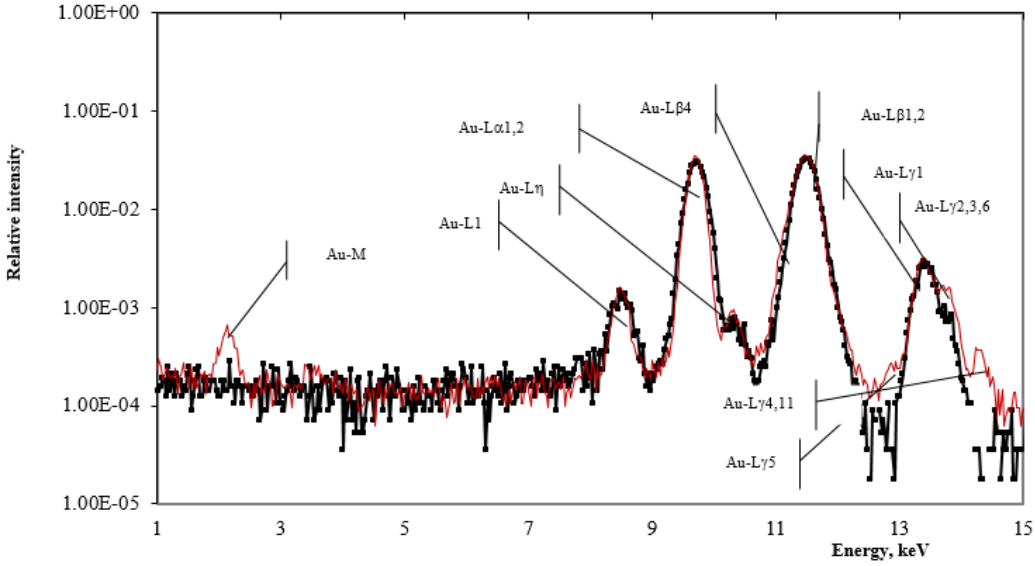

Figure 8. Comparison of simulated (black) and experimental (red) spectra of element Au

Qualitatively, all simulated spectra have Compton scattering bands narrower than the experimental spectra (Figure 7). This is because the MCNP4C2 code has not simulated the Doppler expansion effect for this scattering. This limitation will be fixed in the MCNP5 version (X-5 Monte Carlo Team, 2005).

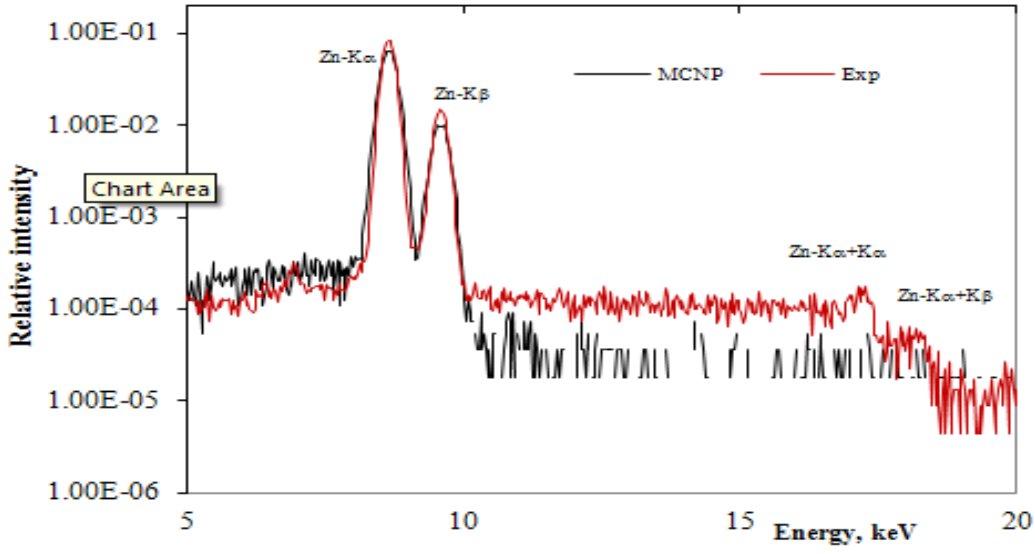

Figure 9. Comparison of simulated and experimental spectra of element Zn

The simulated spectra also show that MCNP4C2 simulates the radiative Auger effect, but with not enough details on energy. Some processes inside the detector and the relevant electronic system, such as pulse pile-up and dead time have not been simulated (Figure 9). As a result, the simulated background is often lower than the experimental one. Moreover, the low energy tail (due to the Auger effect of radiation and inadequate

charge collection) of the K lines in some simulated spectra (Ni, Cu, Zn) is higher than the experimental one. This shows that fluorescence efficiency values ω_K used to construct data for MCPLIB2X are likely to be lower than estimated. In the case of LX emission from element Au, the simulated spectrum (Figure 8) shows the absence of characteristic X-rays of the M, $L_{\gamma 5}$ (L_2-N_1), and $L_{\gamma 11}$ (L_1-N_5, N_6, N_7, L_1-O_1, O_4, O_5, O_6) transitions due to a lack of description in the library and the lack of intensity of the weak lines of the L1 group, such as Lβ4 (L1-M2), Lγ2 (L1-N2), and Lγ3 (L1-N3). This gap was much larger (-80%) than expected (-10%) (Kawrakow & Roger, 2006), mainly due to the nonconformity of the previously mentioned constant primary vacancy probability calculation.

3.2. Simulation of XRF spectra of alloy samples

The XRF spectra of nine gold alloy samples with known concentrations (Table 2) were simulated to evaluate the applicability of the MCNP4C2 code for XRF analysis cases that may be encountered in gold age determinations.

Table 2. Elemental concentrations in Au alloy samples

Sample	Elemental concentration, % (Đõ et al., 2004)					
	Ni	Cu	Zn	Pd	Ag	Au
Au-1					66.91	33.09
Au-2		19.14 ± 0.12			46.62	34.24
Au-3		19.31 ± 0.11		32.28	11.12	37.29
Au-5	9.83	18.95 ± 0.20	3.67 ± 0.12		27.24	40.31
Au-6		8.44 ± 0.18		26.13	13.08	52.35
Au-9	17.23	13.85 ± 0.28	10.18 ± 0.10			58.73
Au-10	13.13	9.12 ± 0.26	2.13 ± 0.07			75.63
Au-11	15.01			10.01		74.99
Au-13		4.71 ± 0.26			3.00	92.29

To avoid the deviations between simulation and experiment caused by differences in geometry and dead time, the element Au was used as an internal standard. The intensity ratio $R_i = K_{\alpha,i}/AuL_{\alpha 1}$ was used to compare the experiment and simulation values. $K_{\alpha,i}$ is the line intensity K_α of element i in the sample, and $AuL_{\alpha 1}$ is the line intensity $L_{\alpha 1}$ of element Au.

The relative deviation between MCNP and Exp is expressed by:

$$\delta_i = \left(R_i(MCNP) - R_i(Exp)\right)/R_i(Exp) \quad (4)$$

The comparison results (Table 3, Figure 10) show that the discrepancy in intensity between simulation and experiment is about 0.02%-26.00%. Particularly for the elements

Pd and Ag, with characteristic X-ray energies > 20 keV corresponding to the low-efficiency region of the detector, the simulated intensity is always 6%-17% greater than the experiment, it is shown that the efficiency of the simulated detector in this region is larger than the efficiency of the real detector. In manufacturing practice, the real detector's active size is not likely to reach the nominal parameters used in the simulation.

Table 3. Relative deviations δ_i between the simulated and experimental results

Sample	δ_i				
	Ni	Cu	Zn	Pd	Ag
Au-1					12.16%
Au-2		3.50%			6.38%
Au-3		19.73%		17.00%	15.57%
Au-5	5.14%	-25.04%	-17.82%		5.92%
Au-6		-26.03%		6.40%	9.69%
Au-9	6.90%	1.29%	12.91%		
Au-10	0.70%	-0.79%	23.82%		
Au-11	0.02%			8.00%	
Au-13		2.06%			8.32%

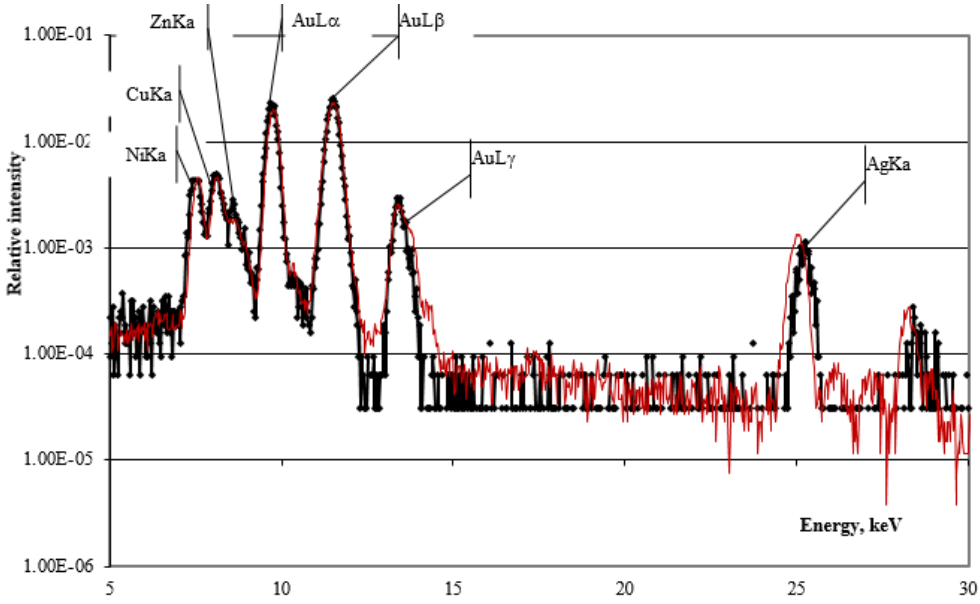

Figure 10. Comparison of simulated (black) and experimental (red) spectra of the Au-5 sample

With the simulated errors in the range of 1%-30%, the modified MCNP4C2 code can be applied to analyze major elements. The simulation can be used for many applications in low concentration analysis that accept errors up to 30%. This MCNP4C2

version is significant for XRF configuration design and helps to evaluate the characteristics of an XRF system even at the design stage, saving time and money before the setup of a new XRF.

4. CONCLUSIONS

The analysis and complement of the source code and library for a modified version of MCNP4C2 have been accomplished. This allows a detailed simulation of the spectral response of conventional XRF systems excited by photons. The code was applied to elemental quantitative analysis in metal samples. These simulations gave relative errors from 0.02% to 26.00%. In addition, the implementation of an XRF configuration in the experiment will be optimized.

ACKNOWLEDGMENTS

The authors would like to express their sincere gratitude to the Institute Project CS/07/01-06 at the Dalat Nuclear Research Institute (VINATOM) for providing financial support to complete this scientific report.

REFERENCES

Đỗ, T. T., Phạm, H. H., Trịnh, T. T. A., Trần, T. H., & Trần, Q. T. (2004). *Nghiên cứu đánh giá hàm lượng các thành phần kim loại trong hợp kim vàng bằng kỹ thuật huỳnh quang tia X* (CS/04/01-05). Viện nghiên cứu Hạt nhân, Viện Năng lượng nguyên tử Việt Nam.

Kawrakow, I. & Roger, D. W. O. (2006). *The EGSnrc code system: Monte Carlo simulation of electron and photon transport* (Technical Report PIRS–701). National Research Council Canada.

LBNL Isotopes Project–Lunds Universitet. (n.d.). *Nuclear data dissemination home page–Atomic data*. http://ie.lbl.gov/toi.htm

Veigele, V. W. J., Briggs, E., Bates, L., Henry, E. M., & Bracewell, B. (1971). X-ray cross-section compilation from 0.1 keV to 1 MeV. *Discussion and results*, *1*(1), 71-431.

Vincze, L., Janssens, K., Vekemans, B., Adams, F., & Lemberge, P. (2004). New Computerisation Methods. In K. Tsuji, J. Injuk, & R. V. Grieken, *X-Ray Spectrometry: Recent Technological Advances* (pp. 435-485). Wiley.

X-5 Monte Carlo Team. (2005). *MCNP–A general Monte Carlo n-particle transport code* (Version 5, Vol.1, LA-UR-03-1987). https://laws.lanl.gov/vhosts/mcnp.lanl.gov/pdf_files/la-ur-03-1987.pdf